*Muhamad Imam Firdaus*[1*], *Ristiyanto Adiputra*[2], *Aditya Rio Prabowo*[3**]

# EMPIRICAL FORMULATION FOR ASSESSING THE ULTIMATE STRENGTH OF SHIP HULL PLATES UNDER GEOMETRICAL IMPERFECTION

# EMPIRIJSKA FORMULACIJA ZA PROCENU ČVRSTOĆE PLOČA BRODSKOG TRUPA U USLOVIMA GEOMETRIJSKE NESAVRŠENOSTI

Originalni naučni rad / Original scientific paper
Rad primljen / Paper received: 06.03.2024
https://doi.org/10.69644/ivk-2025-01-0079

Adresa autora / Author's address:
[1)] Surabaya Merchant Marine Polytechnic, Surabaya 12760, Indonesia M.I. Firdaus https://orcid.org/0000-0001-8550-0482
[*]email: imam.firdaus@poltekpel-sby.ac.id

[2)] Research Center for Hydrodynamics Technology, National Research and Innovation Agency (BRIN), Surabaya 60112, Indonesia R. Adiputra https://orcid.org/0000-0003-3630-9432
[3)] Department of Mechanical Engineering, Universitas Sebelas Maret, Surakarta 57126, Indonesia A.R. Prabowo https://orcid.org/0000-0001-5217-5943 , [**]email: aditya@ft.uns.ac.id

**Keywords**
- plate
- VLCC
- ultimate strength
- initial imperfection
- derived formula

*Abstract*

*The field of ship structure analysis has witnessed considerable progress marked by the proliferation of analytical formulas proposed by researchers as efficient tools for predicting the strength of ship structures, particularly those involving plate configurations. However, a comprehensive review of the existing literature underscores a notable gap - existing studies predominantly focus on a singular aspect, namely plate slenderness when predicting ultimate strength. In a bid to address this limitation and account for the myriad uncertainties inherent in plate structure calculations, this study adopts a nuanced approach. Numerical methods are employed, systematically varying geometric parameters such as b/t ratio and yield strength, alongside introducing initial imperfections in the form of local plate imperfection modes. Further enhancing the analysis complexity, amplitude severity is modified across amplitude, ranging from 25 % to 300 %, encompassing scenarios of slight, average, and severe severity. Leveraging the capabilities of ANSYS® APDL and MATLAB®, an extensive dataset comprising 126 data points is collected and processed. These efforts result in the derivation of a formula tailored for calculating plate normalised strength. Implemented as a quadratic equation, the derived formula demonstrates a remarkable capacity to accurately predict data points characterised by significant deviations. Notably, its performance is gauged against numerical results, revealing a minimal standard error of approximately 0.023. The close alignment observed when comparing the derived formula with recent previous formulas further substantiates its potential as a viable solution for estimating normalised strength, particularly in scenarios influenced by geometric modifications and initial imperfections.*

*Nomenclature*

| Symbols/Name | Units | Description |
|---|---|---|
| $a$ | mm | span length |
| $b$ | mm | bay length |
| $C$ | | constant for amplitude of local imperfection mode |
| $C_0$ | m | amplitude for plate imperfection mode |
| $E$ | MPa | Young's modulus |
| $m$ | | critical half-wave number at span |
| $n$ | | critical half-wave number at bay |
| $r$ | mm | radius of gyration |
| $t$ | mm | plate thickness |

**Ključne reči**
- ploča
- VLCC
- čvrstoća
- početna nesavršenost
- izvedena formula

*Izvod*

*Oblast analize brodske konstrukcije je pokazala značajan napredak okarakterisan razvojem analitičkih formula predloženih od strane istraživača, kao efikasnih alata za procenu čvrstoće brodske konstrukcije, posebno onih sastavljenih iz ploča. Međutim, sveobuhvatan pregled postojeće literature ističe primetan jaz - postojeća istraživanja se pretežno fokusiraju na singularni aspekt, zapravo na vitkost ploče pri oceni čvrstoće. U nastojanjima da se pozabavimo ovim ograničenjem i objasnimo brojne nesigurnosti u proračunima pločastih konstrukcija, u ovom radu se usvaja istančani pristup. Primenjene su numeričke metode uz sistematsko variranje geometrijskih parametara, na primer odnos b/t i napon tečenja, kao i uvođenje početnih nesavršenosti oblika lokalnih nesavršenosti ploče. Analiza se dodatno usložnjava modifikovanjem amplitude u rasponu od 25 % do 300 %, obuhvatajući uslove rada tipa blagi, prosečni i teški. Prednosti ANSYS® APDL i MATLAB® su omogućile prikupljanje i obradu proširenog skupa podataka od 126 tačaka. Time se postiglo izvođenje formule pogodne za izračunavanje normalizovane čvrstoće ploče. Uvedena kao kvadratna jednačina, izvedena formula se pokazala da ima kapaciteta za tačnu procenu podataka sa karakterističnim znatnim odstupanjima. Zapravo, tačnost u odnosu na numeričke rezultate se ogleda u minimalnoj standardnoj devijaciji od oko 0.023. Malo odstupanje se uočava u poređenju izvedene formule sa skorašnjim formulama, čime se dodatno potvrđuje kao potencijalno prihvatljivo rešenje za određivanje normalizovane čvrstoće, posebno u uslovima geometrijskih modifikacija i početnih nesavršenosti.*

| | | |
|---|---|---|
| U | mm | initial displacement |
| $u, x, y, z$ | | element coordinate |
| $W_0$ | mm | maximum value of local imperfection mode |
| $\beta$ | | plate slenderness |
| $\theta$ | ° | rotational displacement |
| $\lambda$ | | column slenderness |
| $\sigma$ | MPa | strength |
| $\sigma_u$ | MPa | ultimate strength |
| $\sigma_y$ | MPa | yield strength |

## INTRODUCTION

Transportation using ships, especially oil tankers, remains one of the primary methods for international oil shipment, spanning from production sites to refineries and ultimately reaching the end consumer points. In the year 2021, shipments of crude oil commodities reached a total of 1.7 billion tons, with oil tanker transportation accounting for 1.2 billion tons, /1/. As shipping activities via oil tankers continue to rise, accidents and failures of oil tankers have become increasingly prevalent and documented. Data from the European Maritime Safety Agency (EMSA) reveals that in the European region, between the years 2014 and 2020, approximately 841 cases of oil tanker accidents occurred /2/. Failures in the structural integrity of oil tankers can be attributed to adverse environmental conditions and extreme circumstances, as well as human errors in ship design and operational practices, /3-4/. The structural failure is attributed to the inability of the hull structure to withstand a certain magnitude of loading, /5-7/. In the broader context, a ship's structural composition can be defined as the amalgamation of continuously stiffened plates, with uniform stiffener spacing between them, /8/.

Numerous studies have been conducted on the large-scale structural aspects of ship hulls, but the focus on the individual plate structure is comparatively limited. Within the realm of structural strength, the integrity of plate elements plays a crucial role. According to Guedes Soares /9/, failure in plate elements occurs when all plates within the structure fail simultaneously. The evaluation of structural failure in ship structures, especially within plates, is commonly gauged through the ultimate strength value of the structure. If the applied load surpasses the ultimate strength value of a system, the system is susceptible to failure /10/. This phenomenon is observed in cases like the Mol, where shipwreck conditions contribute to structural failures in plates, consequently directly reducing ultimate strength and leading to buckling. Zhang et al. /11/ assert that buckling conditions resemble a domino effect, with plate buckling having a significant impact on the overall ship structure. Compressive loading in seaways is one of the aspects that burdens the strength of the plate /12/. Additionally, other factors such as changes in geometry and initial imperfections resulting from the fabrication process necessitate focused attention on plate structures to enhance the strength of ship structures.

Several modifications to the geometric aspects composing the plate can be performed by varying parameters such as the thickness and length of the plate, or a combination of both, commonly denoted as *b/t*, where *b* represents the width of the plate, and *t* signifies the thickness of the plate. Zhang /10/ made modifications to the plate thickness and found a linear correlation between plate thickness and ultimate compressive strength. A similar approach was taken by Zhang and Khan /13/, where they varied the plate thickness from 11.8 mm to 32 mm for plates with a plate aspect ratio of approximately 5. By using the single value critical half-wave in both the longitudinal and transverse directions, they compared the numerical results with the Faulkner equation. In a different case, Kim et al. /14/ collected 315 data points by combining not only geometric aspects such as plate aspect ratio (*a/b*), plate thickness, and material yield, but also aspects of mesh size. Through numerical approaches, a notable aspect highlighted in their research is the significant influence of changing the number of divisions in the mesh when modifying the plate aspect ratio, especially for plates with low thickness levels. This phenomenon is observed not only in flat plates but also in curved plates.

In addition to geometric aspects, uncertainties in real-world conditions allow plates to experience age-related damage, leading to the imperfect state of the structure as built. Residual stresses from welding processes and cracks resulting from incidents are strong contributors to this condition /15-18/. Several studies have demonstrated the significant impact of initial imperfections. A study by Paik /15/ focused on the reduction in ultimate strength in plates with cracks. Beyond cracks, other imperfections such as corrosion were also considered as the factor that can degrade the capability of plate structure to hold such a certain load /12, 19-21/. Khedmati et al. /22/ conducted a study on the ultimate strength of corroded plates by modelling random corrosion, resulting in a significant strength reduction. Furthermore, Bektas /23/ examined the ultimate strength of rectangular plates with variations in aspect ratio and a single value of initial imperfection. The research demonstrated a notable reduction in the ultimate strength of the structure when introducing initial imperfections into the model. While previous studies on initial imperfections often concentrated on larger ship structural elements like stiffened panels, /24-26/, there has been limited exploration of similar imperfections within plate structures. In his study, Xu /27/ considered the presence of half waves along their spans. Consequently, the assessment of the ultimate strength of plates with local imperfection modes has not received extensive attention, particularly regarding their application to structural components and various vessel types.

Currently, research on ship plate structures has delved into numerical approaches validated by experimental results /17, 21/. In addition to these two methods, analytical methods serve as another alternative due to their faster computation time compared to other methods. In the study of plates, various formulas have been formulated to calculate the ultimate strength of plates under the influence of imposed displacement /28-31/. The well-known Faulkner approach /29/ has been a reference in subsequent research, as exemplified by Fujikubo et al. /32/, who compared their numerical results with the Faulkner equation. On another occasion, the formula proposed by Paik et al. /31/ served as a benchmark in the research by Babazadeh and Khedmati /33/, formulating a formula considering crack imperfection. In Table 1, it can be observed that overall, the formulated analytical equations

only consider one geometric aspect, namely plate slenderness. However, as previously explained, there is significant uncertainty beyond geometric aspects, specifically related to initial imperfections. In this study, a new formula is derived based on data obtained from numerical approaches. Geometric aspects are modified by varying the (*b/t*) value, yield strength material, and the degree of severity of the initial imperfection mode. Using the local imperfection mode, the amplitude of initial imperfection is varied at 25 %, 50 %, 75 %, 100 %, 125 %, 150 %, and 300 %, representing slight, average, and severe conditions classified by Smith et al. /34/. A total of 126 data points are analysed using ANSYS APDL® and MATLAB®. The data is processed to derive a new formula, the results of which are verified against formulas from other researchers.

Table 1. Previous proposed formula for plate's ultimate strength.

| Author | Year | Formula |
|---|---|---|
| Frankland | 1940 | $\frac{\sigma_u}{\sigma_y}=\frac{2.25}{\beta}-\frac{1.25}{\beta^2}$ |
| Faulkner | 1975 | $\frac{\sigma_u}{\sigma_y}=\frac{2}{\beta}-\frac{1}{\beta^2}$ |
| Soares | 1988 | $\frac{\sigma_u}{\sigma_y}=\frac{2.16}{\beta}-\frac{1.08}{\beta^2}$ for $\beta>1$ |
| Paik et al. | 2004 | $\frac{\sigma_u}{\sigma_y}=-0.032\beta^4+0.002\beta^2+1.0$ for $\beta\le1.5$<br>$\frac{\sigma_u}{\sigma_y}=\frac{1.274}{\beta}$ for $1.5<\beta\le3.0$<br>$\frac{\sigma_u}{\sigma_y}=\frac{1.248}{\beta^2}+0.283$ for $\beta>3.0$ |

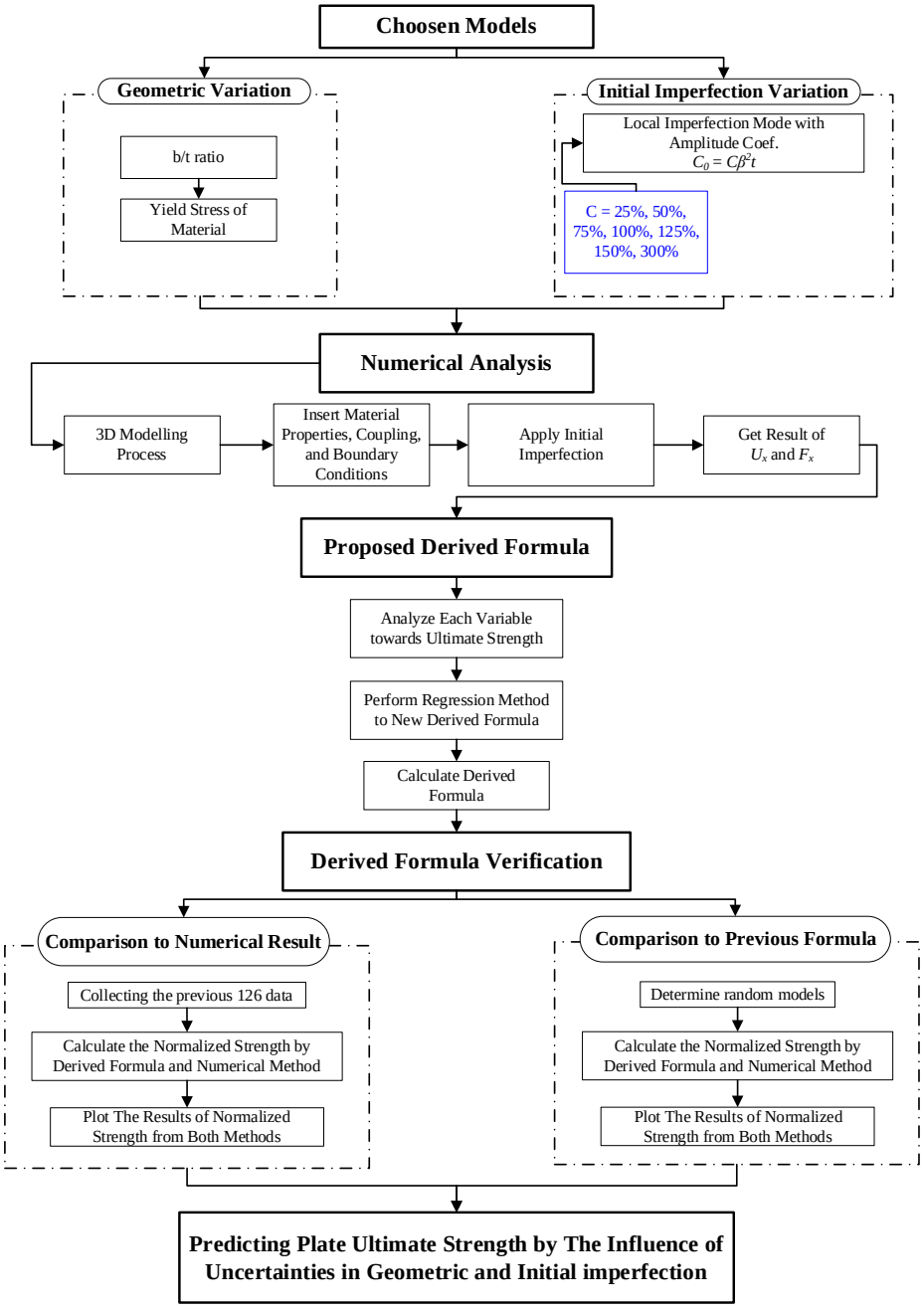


Figure 1. Research flow for predicting plate's ultimate strength.

## METHODOLOGY

### *Flowchart of study*

The selection of selected models was made by choosing specific models that represent the entire geometric variation of the oil tanker plate model.

As illustrated in Fig. 1, the models are varied based on the ratio of *b/t* and the value of yield strength material. Six variations of *b/t* ratio and three variations of yield strength are cross-combined with variations in initial imperfection.

In this study, only the type of local imperfection mode is applied to the model by modifying the coefficient amplitude values. The coefficient value, *C*, representing the constant amplitude of initial imperfection, is multiplied by quadratic plate slenderness and thickness and varied to represent the uncertainty of initial imperfections in actual conditions. Modelling and material properties inputting up to boundary conditions are conducted using ANSYS APDL® software. Meanwhile, MATLAB® is employed to modify model nodes through provided formulas. From each previously varied variable, a comparison is made with the resulting ultimate strength values. For generalisation and ease of comparison, non-dimensional units in the form of normalised strength are applied. Through regression methods, a newly derived formula is generated as an efficient and accurate solution in predicting ultimate strength after statistical verification against numerical results and previously created formulas using random sampling of the model.

### *Plate geometry reference*

In this study, the plate model utilised is derived from the design of a Very Large Crude Carrier (VLCC), based on ISSC-2000 /35/, as illustrated in Fig. 2. The inclusion of both single hull and double hull VLCCs enhances the diversity of the study, allowing for a comprehensive exploration of geometric variations and expanding the scope of potential applications.

a)

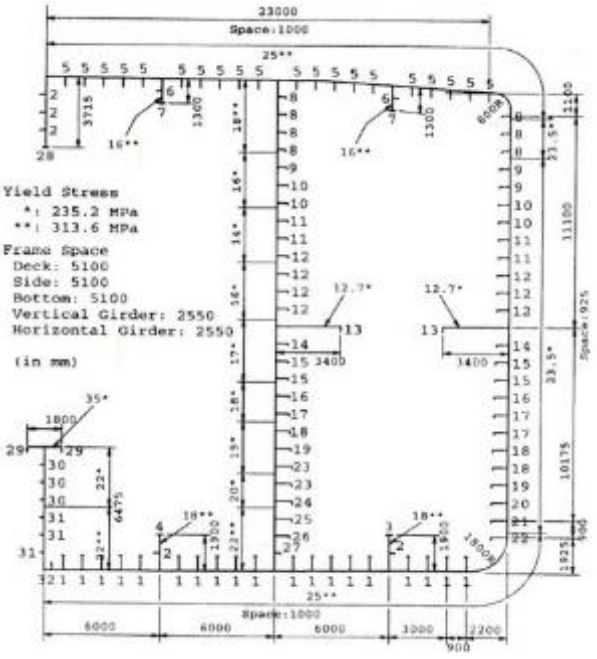


b)

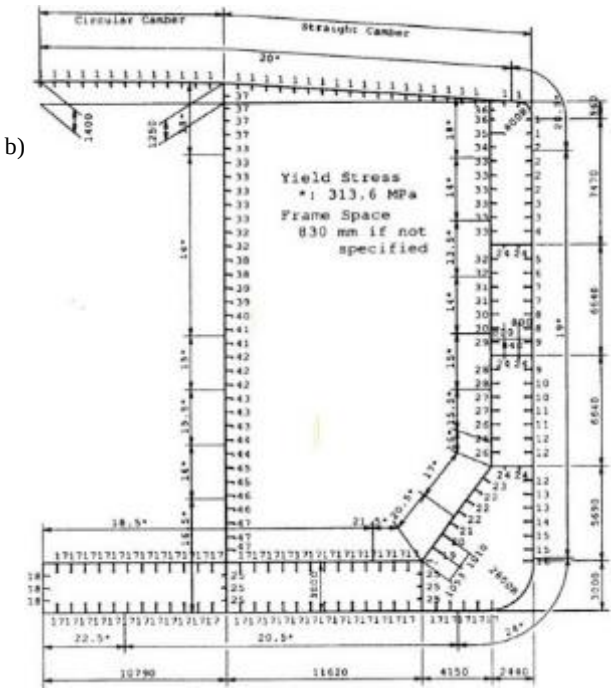


Figure 2. Cross section of: a) single hull VLCC; b) double hull VLCC, /35/.

## CASE CONFIGURATIONS

### *Initial imperfection*

In this study, reference data is obtained from Fujikubo's /36/ research, and this data is intended to determine the imperfection values to be used in the plate model. Based on Smith's studies /34/, three levels of severities are categorised as severe, average, and slight, with variations in their amplitude coefficient. Figure 3 illustrates a plot that represents the relationship between maximum imperfection applied on plate and plate aspect itself. Plate slenderness ratio, in turn, is a function of plate length and thickness, Young's modulus, and yield stress.

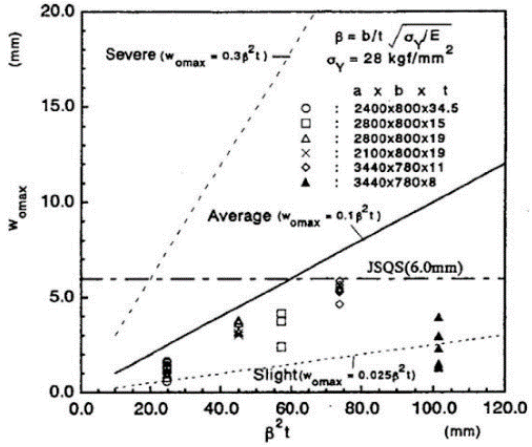


Figure 3. Analysed scatter data of initial geometrical imperfection /36/.

The local plate imperfection mode presented in Eq.(1) is a type of imperfection mode applied in this study, with the formula referencing the work of Adiputra et al. /37/. The amplitude value is represented by $C_0$, which is a function of the coefficient *C* multiplied by the square of the plate slen-

derness ratio and plate thickness. To introduce uncertainty in initial imperfections, the amplitude $C$ is set at 25 %, 50 %, 75 %, 100 %, 125 %, 150 %, and 300 %, representing severity levels from slight to severe. The percentage values alter the given coefficient; for example, at 25 % percentage, the coefficient becomes 0.025, and so forth.

The critical half-wave along the span ($m$) is determined by Eq.(3), where in this case, its values are set to 1. Moreover, along the bay, its value for the entire model is also set as a single value, $n$ = 1. The choice of odd half-wave values is made due to their ability to provide consistent results under both periodic and symmetric boundary conditions, /27/. An illustration of the application of initial imperfections to the model can be seen in Fig. 4.

$$W_0 = C_0 \sin\frac{m\pi x_i}{a}\sin\frac{n\pi y_i}{b}, \quad (1)$$

$$C_0 = C\beta^2 t, \quad (2)$$

$$a/b \le \sqrt{m^2+m}\,. \quad (3)$$

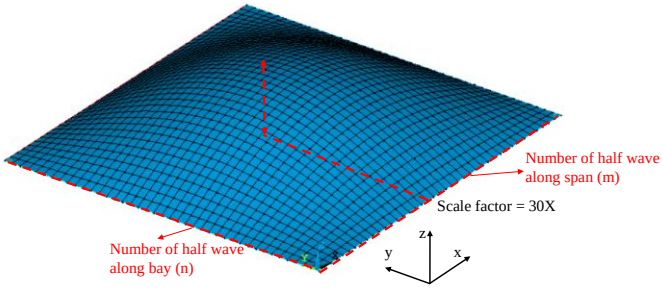


Figure 4. Local imperfection mode illustration.

*Choosing selected models*

Conduct numerical analysis using two reference ship models, the single and double hull VLCCs, and applying various plate geometries can indeed be time-consuming in the analysis. Considering both efficiency and the accuracy of the data obtained, a selection of models is made based on the consideration that the chosen models adequately represent the entire range of plate geometries. As seen in Fig. 5, plate geometries are differentiated by bay length, span, and plate thickness.

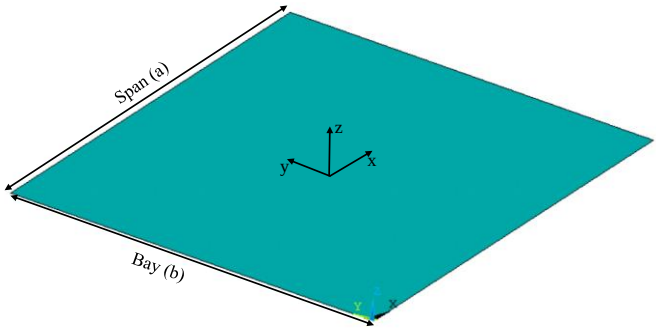


Figure 5. Model illustration of plate.

Therefore, selected models are chosen based on these considerations, as shown in Table 2. In this table, there are 6 models distinguished by the geometry of the plate. The value bay and span equal to 900 mm in the selected models are estimated values that represent the bay length and span in the reference models, as illustrated in Fig. 2. These selected models offer a balance between efficiency and accuracy, covering a representative range of plate geometries for analysis.

Table 2. Selected model definition based on geometrical variations.

| Model | Model geometry ($a$×$b$×t) [mm] | Plate aspect ratio ($a/b$) | $b/t$ ratio |
|---|---|---|---|
| A | 900 × 900 × 25 | 1 | 36 |
| B | 900 × 900 × 23.5 | | 38 |
| C | 900 × 900 × 20 | | 45 |
| D | 900 × 900 × 18 | | 50 |
| E | 900 × 900 × 16 | | 56 |
| F | 900 × 900 × 14 | | 64 |

Additionally, the material characteristics of the plate, for both types of VLCCs, tend to exhibit different tendencies. Therefore, variations are also introduced in yield strength material values. Modifications include adding a variable for yield strength of 352.8 MPa, a value not uncommon in tanker ship types. Consequently, when cross-combined with previously selected 6 different models, there are a total of 18 distinct models based on geometric and material characteristics.

Table 3. Selected model definition based on material yield strength.

| Model | Yield strength [MPa] |
|---|---|
| Low model | 235.2 |
| Medium model | 313.6 |
| High model | 352.8 |

Meanwhile, other material characteristics such as Young's modulus and Poisson's ratio are assumed to be the same, as presented in Table 4.

Table 4. Plate material characteristics.

| Material properties [units] | Value |
|---|---|
| Young's modulus [MPa] | $2.06 \times 10^5$ |
| Poisson's ratio | 0.3 |

To provide a clearer explanation that the selected models represent other models, plots in Figs. 6 and 7 are presented. In Fig. 6, comparison is made on column slenderness ratio properties against plate thickness. Column slenderness is one of the geometric parameters considered in ship structure modelling, representing a function of span, radius of gyration, yield strength, and Young's modulus, is shown in Eq.(4).

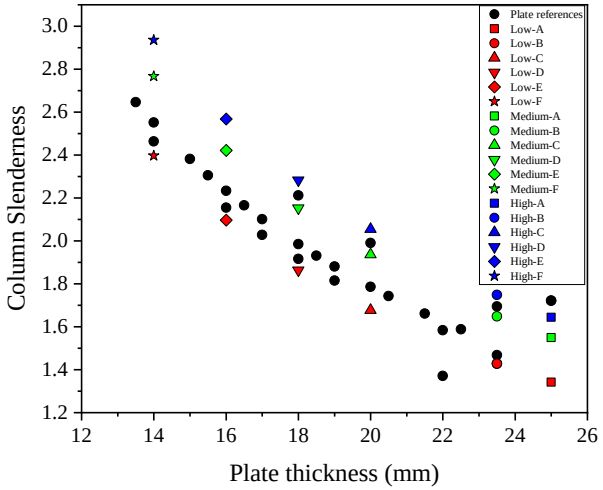


Figure 6. Comparison between column slenderness and plate thickness.

$$\lambda = \frac{a}{\pi r}\sqrt{\frac{\sigma_y}{E}}\,. \tag{4}$$

Meanwhile, in Fig. 7, a comparison between column slenderness and plate slenderness ratio is provided. In both graphs, all selected models represent the highest to lowest values for these three parameters. In the verification step of the newly derived formula, plate reference models are used to validate the accuracy of calculated predictions. This ensures that the new formula accurately represents the behaviour observed in the plate reference models.

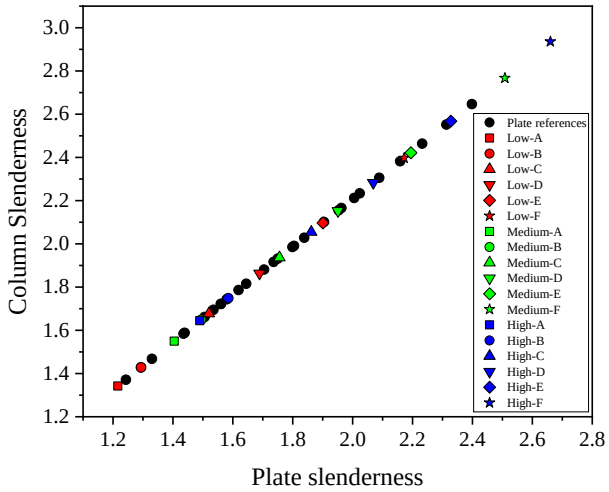


Figure 7. Comparison between column and plate slenderness.

*Numerical analysis setting*

The analysed plate in this study is located between stiffeners, as depicted in Fig. 8. Boundary conditions applied to the plate are adapted from the conditions Anyfantis /38/, provided for stiffened panels. The difference in the current study is that there are no constraints applied to the web or the middle section of the plate. Instead, specific fix constraints are applied to the entire edge, as illustrated in Fig. 9. Only the edge portion is subjected to imposed displacement with a uniform condition, allowing nodes in that area to move together when displacement is applied. This boundary condition setup aims to simulate the conditions of a plate located between stiffeners, ensuring a representative analysis of the plate's behaviour within the given structural context.

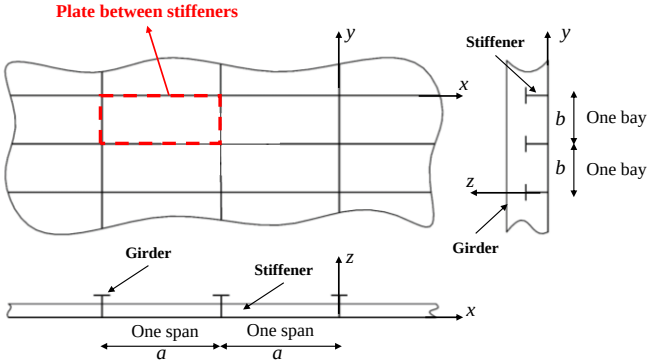


Figure 8. Plate location.

Referring to the research by Hanif et al. /39/ and following the guidelines from Kohnke /40/, the '181' shell element and bilinear isotropic hardening are chosen for this analysis because they sequentially provide appropriate modelling conditions and accurately represent material response when subjected to loads. The mesh configuration on the plate is then varied, as illustrated in Fig. 10. For all models, the number of mesh divisions in the *x*-axis × *y*-axis is set to 40 × 40. This mesh configuration aims to study the sensitivity of the analysis to mesh density and ensure that the chosen mesh adequately captures plate behaviour under applied conditions.

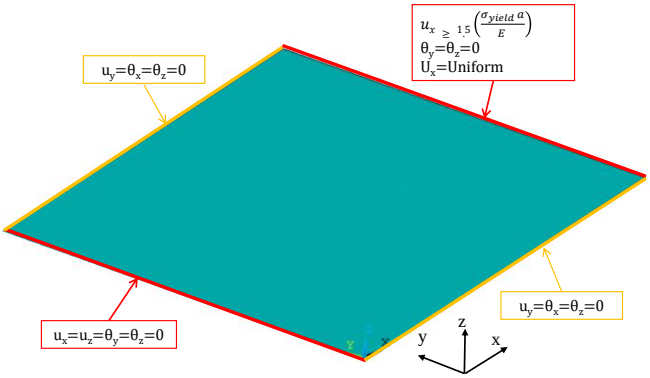


Figure 9. Applied boundary condition on plate model.

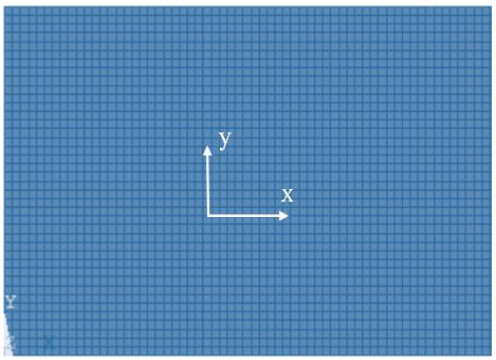


Figure 10. Plate illustration after mesh setting applied.

## RESULT AND DISCUSSION

*Geometrical variations effect*

The influence exerted by variations in geometric aspects shows significant results. In Fig. 11a, the effect of increase in *b/t* ratio is capable of decreasing the ultimate strength. As observed in the graph, a significant decline occurs. This decrease is attributed to the impact of reducing plate thickness, which affects the plate slenderness value. As previously known, plate slenderness is one of the variables influencing the local plate imperfection mode, triggering plate collapse. Hence, in this study, it can be observed that a decrease in *b/t* ratio corresponds to a proportional effect on the ultimate strength of the plate.

In addition to the geometric shape of model, the effect of material characteristics also plays a significant role. Although Fig. 11b demonstrates that an increase in plate yield strength results in an increase in ultimate strength, the opposite is shown in terms of normalised strength. This indicates that even though there is an increase in ultimate strength, raising the yield strength value needs to be considered to effectively impact the structural strength of the plate. Similar to the previous variation, the effect of yield strength itself is relatively constant concerning normalised strength, in this case, from

the A to the F model. This implies that, in certain cases, an increase in yield strength may not translate proportionally to an increase in structural efficiency of the plate, emphasising the need for a balanced consideration of various factors in material selection.

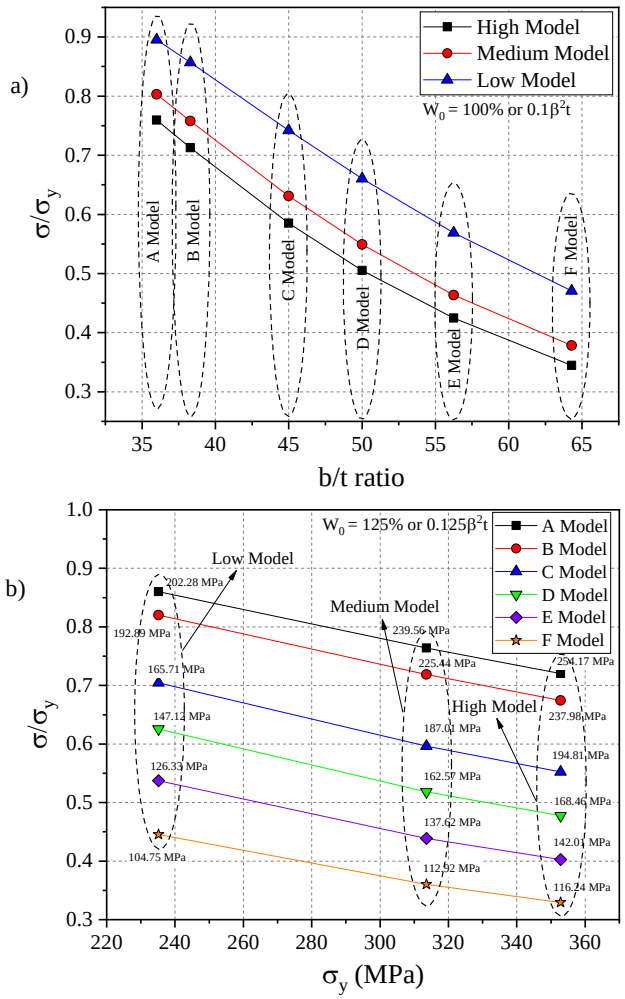


Figure 11. Effect of different geometric parameter on ultimate strength: a) *b/t* ratio; b) yield strength of material.

*Initial imperfection variations effect*

In the case of an increase in the amplitude of initial imperfection, there is a decrease in ultimate strength value, as can be seen in Fig. 12. This decrease is particularly significant in models with low plate thickness, such as the D, E, and F models. In models A and B, the normalised strength decrease in amplitude imperfection from 150 to 300 % is observed to be approximately less than 1.5. Conversely, in all three models with the lowest plate thickness, the difference exceeds 2. Although Eq.(2) elucidates the influence of plate geometry on the magnitude of imperfection values, specific values of plate thickness and initial imperfection amplitude have a pronounced effect on the strength of the plate structure. It is crucial to consider these variations in response to initial imperfections based on specific characteristics of the plate being analysed.

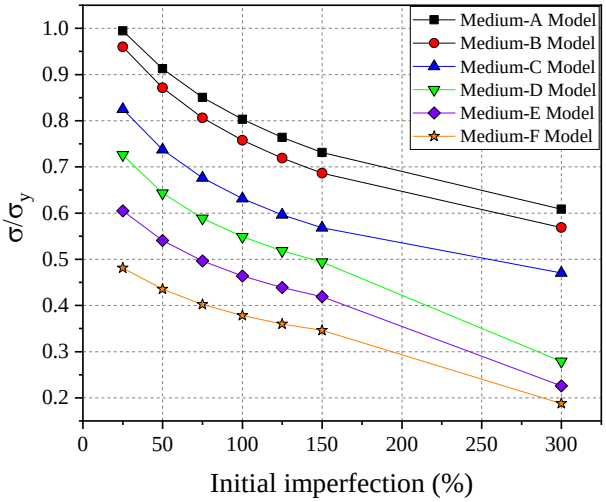


Figure 12. Influence of initial imperfection on normalised strength.

## DERIVED FORMULA

*Analysing each plate parameter towards normalised strength value*

Before deriving the formula, an evaluation of the influence of each varied variable on the normalised strength is necessary. Table 5 presents a statistical approach to measure the influence of each variable. In the table, plate and column slenderness ratio have the largest T-value of -15.950 and -15.947, respectively. The negative value indicates that any increase in those ratios has an opposite effect or a decrease in normalised strength in general. With a confidence level of 95 %, all modified parameters show a significant impact on any change in normalised strength. This is evidenced by significance values for each parameter being smaller than the significance level in the table, which is 0.05. These statistical results affirm that each modified parameter significantly influences the changes in normalised strength.

Table 5. Statistical analysis of each variable effect on ultimate strength value.

| Parameter | T-value | Significance | T-Table | Significance level |
|---|---|---|---|---|
| *b/t* ratio | -13.220 | < 0.001 | ±1.966 | 0.05 |
| $\beta$ | -15.950 | < 0.001 | | |
| $\lambda$ | -15.947 | < 0.001 | | |
| Yield strength | -3.536 | < 0.001 | | |
| Initial imperfection | -7.119 | < 0.001 | | |

In addition to conducting statistical calculations, the correlation between each variable, both geometrical and initial imperfection aspects, are also explored through graphical plotting. In Fig. 13a to 13e, overall, the graphs show an inversely proportional linear relationship with normalised strength. However, in Fig. 13c, the middle line in some box charts provides data that the median of normalised strength is not always linear. The median line in that graph indicates fluctuations. Additionally, in Fig. 13a and d, several data points fall outside the box chart range, especially beyond the 95$^{th}$ percentile. Therefore, in this study, the derivation of the formula does not use a linear but a nonlinear equation in the form of a polynomial equation to capture deviations that occur in each data point across various parameter variations.

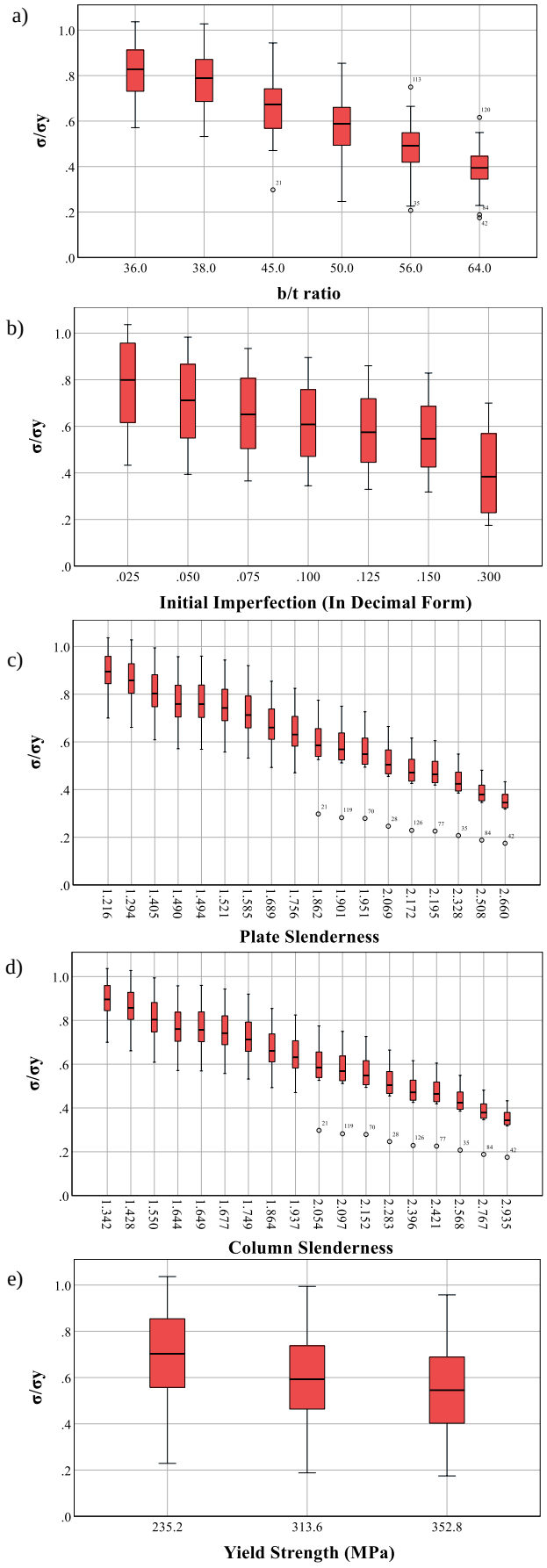


Figure 13. Data range of normalised strength influence by numerous parameters.

These nonlinear equations, specifically polynomial equations, provide a more flexible and adaptable framework to model the complex relationships observed in the data, accounting for fluctuations and variations that may not be adequately captured by linear equations.

*Proposed derived formula for $\sigma_u/\sigma_y = f(\beta,\lambda,C)$*

Based on the comparison of the influence of each variable on normalised strength, variables such as plate slenderness and initial imperfection are independent variables in the equation for normalised strength, as shown in Eq.(5). The value of *b/t* ratio itself has been represented by plate slenderness as they have a similar approach. Additionally, in the form of a normalised strength function (rather than ultimate strength), the yield strength is automatically considered, even if not explicitly stated in the equation. With fewer variables, the equation becomes more efficient and compact,

$$\frac{\sigma_u}{\sigma_y} = f(\beta,\lambda,C)\cdot \tag{5}$$

This simplified equation captures the essential factors influencing normalised strength while maintaining efficiency and conciseness. The reduced number of variables enhances the practicality and interpretability of the equation.

Through the regression method, the 126 data points previously calculated via the numerical method are processed. As can be seen in Table 6 by aiming for three independent variables, a quadratic equation is generated with an $R^2$ value reaching 0.986. A value of 0.986 indicates that the three independent variables accurately represent results compared to numerical results at 98.6 %. As explained earlier, the selected equation is quadratic, not linear, because it can capture data points beyond the 95$^{th}$ percentile range. This quadratic equation provides a more accurate representation of the complex relationship between the variables and normalised strength, especially capturing the deviations in data points beyond the 95$^{th}$ percentile range.

Table 6. Summary regression analysis findings.

| Constant | Coefficient | | | | | $R^2$ | Adj. $R^2$ |
|---|---|---|---|---|---|---|---|
| | $\beta^2$ | $\beta^2\lambda^2$ | $\beta$ | $C^2$ | $C$ | | |
| 1.505 | -0.173 | 0.011 | -0.141 | 3.129 | -2.337 | 0.986 | 0.986 |

Based on the equation and statistical data generated in Table 6, they are organised to produce a new derived formula for calculating normalised strength on a plate, as demonstrated in Eq.(6). The negative value for plate slenderness and initial imperfection amplitude indicate a negative influence on the increase in normalised strength. To extend the coverage to data beyond the range, the terms $\beta^2$ and $C^2$ play a role in reaching these data points to improve the accuracy of the results,

$$\frac{\sigma_u}{\sigma_y} = 1.505 - 0.173\beta^2 + 0.011\beta^2\lambda^2 - 0.141\beta + \\ +3.129C^2 - 2.337C\cdot \tag{6}$$

This derived formula allows for the prediction of normalised strength on a plate based on the specified parameters, providing a more flexible and accurate tool for understanding the relationship between these variables and the plate's structural response.

*Verification derived formula for $\sigma_u/\sigma_y = f(\beta,\lambda,C)$*

Data verification and validation are conducted twice in this study. In the first validation, the data are re-examined against numerical calculations, as illustrated in Fig. 14. The diagonal axis represents the alignment of calculation results with the derived formula in Eq.(6). Meanwhile, the vertical axis indicates the results of numerical calculations for the previous 126 data points. With a standard error of only 0.023, the graph demonstrates a high level of consistency between the two calculation models. This is further evidenced by numerous numerical calculation results aligning closely with the diagonal line. The standard error value itself is obtained from the square root calculation of 1 minus the adjusted $R^2$, multiplied by the standard deviation value of the data.

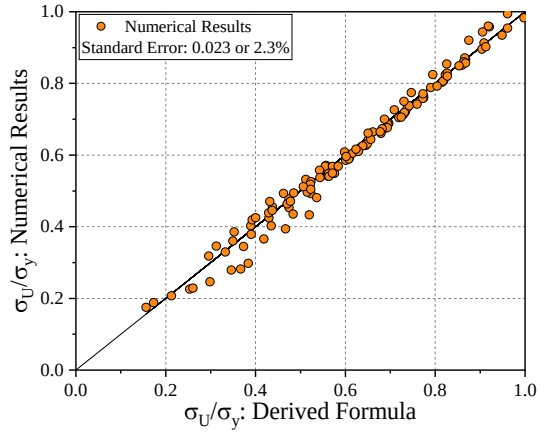


Figure 14. Validating by comparing to numerical results.

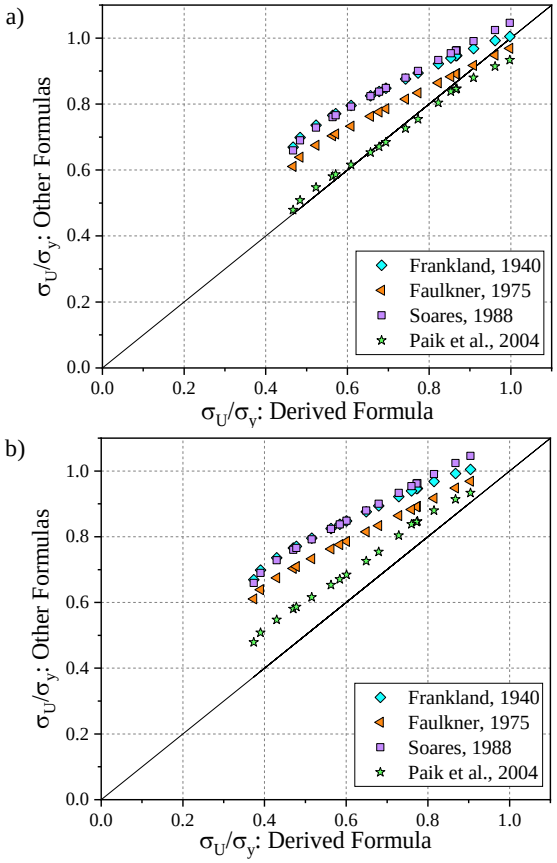


Figure 15. Validating first derived formula by comparing to previous formulas: a) at $C = 0.05$; b) at $C = 0.1$.

The second and final validation involves a comparison of results obtained from the developed derived formula with various formulas previously published by earlier researchers. In contrast to the preceding graph, the vertical axis below illustrates the computed values using formulas referenced in Table 1. For this comparison, the amplitude of the initial imperfection is assumed to have values at 50 % or 0.05, and 100 % or 0.1. Upon examination of Fig. 15, both 15a and 15b, the results derived from the developed formula exhibit a trend similar to most recently proposed formulas, particularly those by Paik et al. /31/.

In both graphs, the calculations from the well-known Faulkner /29/ also provide an approach that is nearly identical to the current derived formula, with minimal differences in values. However, in the graph with an initial imperfection amplitude equal to 100 % or 0.1, the calculations from the derived formula slightly underestimate. This discrepancy may arise due to the influence of initial imperfection variable and differences in the boundary condition approach.

## CONCLUSIONS

The current study on plate ultimate strength involves the variation of *b/t* ratio, yield strength, and initial imperfections in the form of local plate imperfection modes. These variations directly influence other geometric aspects in the form of plate and column slenderness ratio. Through numerical simulations, results are processed to derive a compact formula, enabling the prediction of normalised plate strength values.

- Variations in *b/t* ratio, yield strength, and initial imperfections significantly impact both ultimate and normalised strength values.
- Modifications to yield strength exhibit a direct relationship with changes in ultimate strength but an inverse relationship with normalised strength.
- At specific values of plate thickness and initial imperfection amplitude, there is a significant alteration in normalised strength.
- The quadratic equation form effectively captures data with significant deviations, thereby enhancing prediction accuracy compared to linear equation formulas.
- Future studies could be extended by introducing more variations in types of imperfection modes, such as hungry horse mode or degradation of yield strength due to residual stress.

## REFERENCES

1. United Nations Conference on Trade and Development, Review of Maritime Transport, United Nations, Geneva, 2022.
2. Annual Overview of Marine Casualties and Incidents 2022, European Maritime Safety Agency, 2022.
3. Parunov, J., Rudan, S., Bužančić Primorac, B. (2017), *Residual ultimate strength assessment of double hull oil tanker after collision*, Eng. Struct. 148: 704-717. doi: 10.1016/j.engstruct.2017.07.008
4. Buzančić Primorac, B., Parunov, J. (2015), *Structural reliability assessment of accidentally damaged oil tanker*, In: C. Guedes Soares, R. Dejhalla, D. Pavletic (Eds.), Towards Green Marine Technology and Transport, 1st Ed, CRC Press, London, 2015. EISBN 9780429225604
5. Matos Luís, R.J.A., Hussein, A.W.A., Guedes Soares, C. (2007), *On the effect of damage to the ultimate longitudinal strength of double hull tankers*, Proc. 10th Int. Symp. on Practical Design of Ships and Other Floating Structures (PRADS'07), American Bureau of Shipping, Houston, Texas, USA.

6. Hussein, A.W., Guedes Soares, C. (2009), *Reliability and residual strength of double hull tankers designed according to the new IACS common structural rules*, Ocean Eng. 36(17-18): 1446-1459. doi: 10.1016/j.oceaneng.2009.04.006
7. Prestileo, A., Rizzuto, E., Teixeira, A.P., Soares, C.G. (2013), *Bottom damage scenarios for the hull girder structural assessment*, Marine Struct. 33: 33-55. doi: 10.1016/j.marstruc.2013.0 4.001
8. Cui, W., Wang, Y., Pedersen, P.T. (2002), *Strength of ship plates under combined loading*, Marine Struct. 15(1): 75-97. doi: 10.1 016/S0951-8339(01)00009-0
9. Guedes Soares, C. (1992), *Design equation for ship plate elements under uniaxial compression*, J Constr. Steel Res. 22(2): 99-114. doi: 10.1016/0143-974X(92)90010-C
10. Zhang, S. (2016), *A review and study on ultimate strength of steel plates and stiffened panels in axial compression*, Ships Offshore Struct. 11(1): 81-91. doi: 10.1080/17445302.2014.99 2610
11. Zhang, Y., Huang, Y., Zhang, Q., Liu, G. (2016), *Ultimate strength of hull structural plate with pitting corrosion damnification under combined loading*, Ocean Eng. 116: 273-285. doi: 10.1016/j.oceaneng.2016.02.039
12. Silva, J.E., Garbatov, Y., Guedes Soares, C. (2013), *Ultimate strength assessment of rectangular steel plates subjected to a random localised corrosion degradation*, Eng. Struct. 52: 295-305. doi: 10.1016/j.engstruct.2013.02.013
13. Zhang, S., Khan, I. (2009), *Buckling and ultimate capability of plates and stiffened panels in axial compression*, Marine Struct. 22(4): 791-808. doi: 10.1016/j.marstruc.2009.09.001
14. Kim, D.K., Ban, I., Poh, B.Y., Shin, S.C. (2023), *A useful guide of effective mesh-size decision in predicting the ultimate strength of flat- and curved plates in compression*, J Ocean Eng. Sci. 8 (4): 401-417. doi: 10.1016/j.joes.2022.02.014
15. Paik, J.K., Kumar, Y.V.S., Lee, J.M. (2005), *Ultimate strength of cracked plate elements under axial compression or tension*, Thin-Walled Struct. 43(2): 237-272. doi: 10.1016/j.tws.2004.0 7.010
16. Li, D., Feng, L., Xiao, W. (2020), *A study on residual ultimate strength of steel unstiffened plate with a crack*, Appl. Ocean Res. 103: 102336. doi: 10.1016/j.apor.2020.102336
17. Paik, J.K. (2008), *Residual ultimate strength of steel plates with longitudinal cracks under axial compression-experiments*, Ocean Eng. 35(17-18): 1775-1783. doi: 10.1016/j.oceaneng.2008.08.012
18. Paik, J.K. (2009), *Residual ultimate strength of steel plates with longitudinal cracks under axial compression-Nonlinear finite element method investigations*, Ocean Eng. 36(3-4), 266-276. doi: 10.1016/j.oceaneng.2008.12.001
19. Ahmmad, M.M., Sumi, Y. (2010), *Strength and deformability of corroded steel plates under quasi-static tensile load*, J Marine Sci. Technol. 15(1): 1-15. doi: 10.1007/s00773-009-0066-1
20. Rahbar-Ranji, A. (2012), *Ultimate strength of corroded steel plates with irregular surfaces under in-plane compression*, Ocean Eng. 54: 261-269. doi: 10.1016/j.oceaneng.2012.07.030
21. Zhang, Y., Huang, Y., Wei, Y. (2017), *Ultimate strength experiment of hull structural plate with pitting corrosion damage under uniaxial compression*, Ocean Eng. 130: 103-114. doi: 10. 1016/j.oceaneng.2016.11.065
22. Khedmati, M.R., Nouri, Z.H.M.E., Roshanali, M.M. (2012), *A comparative computational investigation on the effects of randomly distributed general corrosion on the post-buckling behaviour of uniaxially loaded plates*, J Mech. Sci. Technol. 26(3): 767-783. doi: 10.1007/s12206-011-1222-1
23. Bektas, N.B. (1999), *The effects of aspect ratio and initial imperfection shape on the uniaxial plate strength*, J Eng. Sci. 5(1): 911-919.
24. Georgiadis, D.G., Samuelides, M.S., Li, S., et al. (2021), *Influence of stochastic geometric imperfection on the ultimate strength of stiffened panel in compression*, In: J. Amdahl, C. Guedes Soares (Eds.), Developments in the Analysis and Design of Marine Structures, Proc. 8th Int. Conf. on Marine Structures (MARSTRUCT 2021, June 2021, Trondheim, Norway), 1st Ed. CRC Press, London, 2021. EISBN 9781003230373
25. Gandhi, P.R., Doshi, K., Vhanmane, S. (2012), *Ultimate strength analysis of stiffened plates with initial imperfections*, Int. J Innov. Res. Devel. 1(10) Sp. Issue: 190-206.
26. Shi, X.H., Zhang, J., Soares, C.G. (2018), *Numerical assessment of experiments on the ultimate strength of stiffened panels with pitting corrosion under compression*, Thin-Walled Struct. 133: 52-70. doi: 10.1016/j.tws.2018.09.029
27. Xu, M.C., Yanagihara, D., Fujikubo, M., Guedes Soares, C. (2013), *Influence of boundary conditions on the collapse behaviour of stiffened panels under combined loads*, Marine Struct. 34: 205-225. doi: 10.1016/j.marstruc.2013.09.002
28. Frankland, J.M. (1940), *The strength of ship plating under edge compression*, US EMB Navy Yard, Washington D.C., Report, 469: 28p.
29. Faulkner, D. (1975), *A review of effective plating for use in the analysis of stiffened plating in bending and compression*, J Ship Res. 19(1): 1-17. doi: 10.5957/JSR.1975.19.1.1
30. Soares, C.G. (1988), *Design equation for the compressive strength of unstiffened plate elements with initial imperfections*, J Constr. Steel Res. 9(4): 287-310. doi: 10.1016/0143-974x(88)90065-x
31. Paik, J.K., Thayamballi, A.K., Lee, J.M. (2004), *Effect of initial deflection shape on the ultimate strength behavior of welded steel plates under biaxial compressive loads*, J Ship Res. 48 (01): 45-60. doi: 10.5957/jsr.2004.48.1.45
32. Fujikubo, M., Yao, T., Khedmati, M.R. (1999), *Estimation of ultimate strength of ship bottom plating under combined transverse thrust and lateral pressure*, J Soc. Naval Arch. Japan, 1999(186): 621-630. doi: 10.2534/jjasnaoe1968.1999.186_621
33. Babazadeh, A., Khedmati, M.R. (2019), *Empirical formulations for estimation of ultimate strength of cracked continuous unstiffened plates used in ship structure under in-plane longitudinal compression*, Eng. Fail. Anal. 100: 470-484. doi: 10.1016/j.eng failanal.2019.02.051
34. Smith, C.S., Davidson, P.C., Chapman, J.C. (1988), *Strength and stiffness of ships' plating under in-plane compression and tension*, Royal Inst. Naval Arch. Trans. 130: 20p. ISSN 0035-8967
35. Ohtsubo, H., Sumi, Y. (Eds.), Proc. 14th Int. Ship and Offshore Structures Congress, 1st Ed., Elsevier Science, Oxford, United Kingdom, 2000. ISBN 0080436021
36. Fujikubo, M., Yao, T., Khedmati, M.R., et al. (2005), *Estimation of ultimate strength of continuous stiffened panel under combined transverse thrust and lateral pressure Part 1: Continuous plate*, Marine Struct. 18(5-6): 383-410. doi: 10.1016/j.marstruc. 2005.08.004
37. Adiputra, R., Yoshikawa, T., Erwandi, E. (2023), *Reliability-based assessment of ship hull girder ultimate strength*, Curved Layered Struct. 10(1): 20220189. doi: 10.1515/cls-2022-0189
38. Anyfantis, K.N. (2020), *Ultimate strength of stiffened panels subjected to non-uniform thrust*, Int. J Naval Arch. Ocean Eng. 12: 325-342. doi: 10.1016/j.ijnaoe.2020.03.003
39. Hanif, M.I., Adiputra, R., Prabowo, A.R., et al. (2023), *Assessment of the ultimate strength of stiffened panels of ships considering uncertainties in geometrical aspects: Finite element approach and simplified formula*, Ocean Eng. 286: 115522. doi: 10.1016/j.oceaneng.2023.115522
40. Kohnke, P. (Ed.), ANSYS Theory Reference-Release 5.6. ANSYS, SAS IP, Inc., 1999.